Chemistry–A European Journal
Research Article
doi.org/10.1002/chem.202403166
Chemistry Europe
European Chemical Societies Publishing
www.chemeurj.org

The Effect of Hyperconjugation and Hydrogen Bonding on the Conformers of Methylated Monosaccharides

Juliette C. Whiteside,[a] Aran Insausti,[a, b, c] Jiarui Ma,[a] Arsh S. Hazrah,[a, d] Wolfgang Jäger,[a] and Yunjie Xu*[a]

The conformational landscapes of four 1-O-methylated monosaccharides—methyl α-glucose, methyl β-glucose, methyl α-galactose, and methyl β-galactose—were characterized using jet-cooled broadband rotational spectroscopy, supported by density functional theory calculations. A newly designed, simple pulsed nozzle assembly was used to introduce the sugar samples into a jet expansion without thermal degradation, eliminating the need for a complex and expensive laser ablation system. Ten conformers were experimentally identified by assigning their rotational spectra, and the intricate methyl internal rotation splittings were analysed. Notably, methylation alters the directionality of intramolecular hydrogen bonding of α-galactose highlighting its impact on structural preference. Natural bond orbital, intrinsic bond strength, and non-covalent interaction analyses were conducted to explore the interplay between hydrogen bonding and hyperconjugation. A set of σ to σ* neutral hyperconjugative interactions was found to override a strong hydrogen bond, driving a preference for the gauche conformers.

Introduction

Carbohydrates are ubiquitous in molecular biology and play an important role in energy storage and in molecular recognition.[1] While conformational properties of carbohydrates are widely recognized to play an essential role in glycan recognition events,[2,3] detailed experimental conformational analyses are rarely available.[4] This partly stems from the lack of a straightforward spectroscopic technique that can assess subtle conformational differences related to OH orientations in these highly flexible systems with abundant OH groups. While theoretical modelling has been crucial for elucidating non-covalent interactions and conformational structures of carbohydrates,[5] a significant challenge is the lack of high-quality experimental data that can clearly distinguish only subtly different conformations for benchmarking the commonly used theoretical approaches. This is the case even for simple monosaccharides[6] which contain several OH groups capable of forming complicated intra- and intermolecular hydrogen bonding networks, and which act as a playground for various σ to σ* hyperconjugative (also called neutral hyperconjugative) interactions.[7] To better predict the net effect of the compounding stereoelectronic effects, definitive experimental conformational preference data are invaluable.[2]

Jet-cooled rotational spectroscopy, especially chirped-pulse Fourier transform microwave (CP-FTMW) spectroscopy,[8] has emerged as a powerful spectroscopic technique to provide very detailed information about molecular structures, including subtle OH orientations[9] and minor ring puckering conformations.[10] Using rotational spectroscopy in combination with laser ablation, conformers of a number of monosaccharides, for example, α/β-D-glucose (Glc),[11] α-D-galactose (Gal),[12] and β-D-allose,[13] as well as two different anomers of 2-deoxy-D-riboside[14] have been observed in their isolated state, unbiased by solvent interactions. Although solvents can influence conformational behaviour, these gas-phase studies provide decisive, detailed insights into hydrogen-bonding networks and ring conformations—information rarely obtainable through other spectroscopic techniques—offering high-quality data for theoretical benchmarking.

In this paper, we explore conformational panoramas of four 1-O-methylated monosaccharides (Figure 1), namely methyl α-D-glucopyranoside (Me-α-Glc), methyl β-D-glucopyranoside (Me-β-Glc), methyl α-D-galactopyranoside (Me-α-Gal), and methyl β-D-galactopyranoside (Me-β-Gal) in their isolated state using rotational spectroscopy in conjunction with extensive theoretical modelling. Methylated carbohydrates are modifications found in nature and are also extensively used in synthetic carbohydrate chemistry as a

[a] J. C. Whiteside, A. Insausti, J. Ma, A. S. Hazrah, W. Jäger, Y. Xu
Department of Chemistry, University of Alberta, 11227 Saskatchewan Dr NW, T6G 2G2 Edmonton, AB, Canada
E-mail: yunjie.xu@ualberta.ca
[b] A. Insausti
Departamento de Química Física, Facultad de Ciencia y Tecnología,Universidad del País Vasco (UPV-EHU), 48080 Bilbao, Spain
[c] A. Insausti
Biofisika Institute (CSIC, UPV/EHU), Universidad del País Vasco (UPV-EHU), 48080 Bilbao, Spain
[d] A. S. Hazrah
Department of Molecular Spectroscopy, Max Planck Institute for Polymer Research,Ackermannweg 10, 55128 Mainz, Germany

Supporting information for this article is available on the WWW under https://doi.org/10.1002/chem.202403166

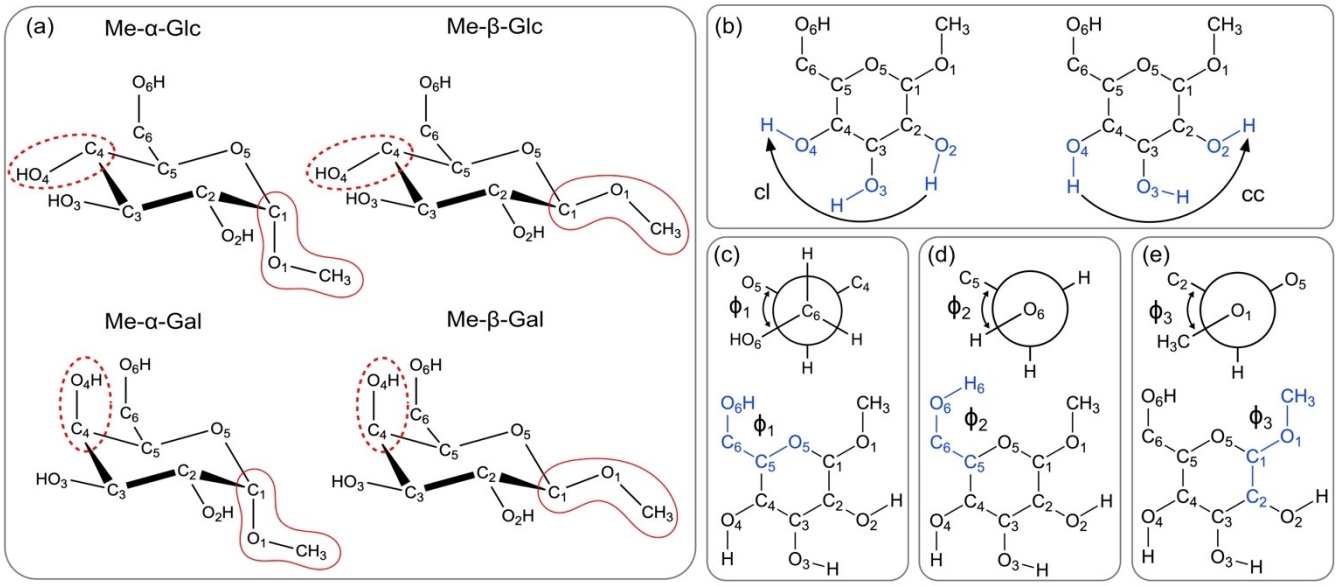

Figure 1. (a) The $^4C_1$ chair conformations of α- and β–anomers of methyl glucose and methyl galactose. While the solid red lines indicate the difference between α- and β-anomers, the dashed red lines highlight the difference between Me-Glc and Me-Gal. (b) The clockwise (cl) and counterclockwise (cc) hydrogen bonding networks. Since the O2–H, O3–H, and O4–H groups of the cyclic hexoses adopt a concerted orientation, the torsional angles involving these groups are not labelled explicitly. (c) Newman projections (top) and backbone designations (bottom) of Φ_1, the O6–C6–C5–O5 torsional angle. The possible values of Φ_1 are +60°, −60°, and 180° are labelled as G+, G-, and T, respectively. (d) Newman projection of Φ_2, the H6–O6–C6–C5 torsional angle. The possible values of Φ_2 are +60°, −60°, and 180° are labelled as g+, g-, and t. (e) Newman projection of Φ_3, CH3–O1–C1–C2 torsional angle. The possible values of +60°, −60°, and 180° are labelled as G+, G-, and T, respectively.

common intermediate and to steer reaction products.[15] While not much is known about the specific function of methylation in living organisms, it is generally acknowledged that methylation can influence intra- and intermolecular hydrogen bonding networks and as such play a key role in glycan recognition processes.[2,3]

We aim to achieve three main objectives in this study. First, we demonstrate that using a newly designed nozzle cap allows for detecting rotational spectra of these monosaccharides with high sensitivity, eliminating the need for an expensive laser ablation system. Second, we illustrate the experimental conformational preferences of these methylated monosaccharides in the gas phase, providing a rare opportunity to directly compare the intramolecular hydrogen bonding networks with those of the corresponding unmethylated monosaccharides. Finally, we sought to understand how methylation exerts its influence on the stereoelectronic effects and hydrogen bonding networks of monosaccharides through both experimental data and theoretical modelling.

Results and Discussion

Conformational Searches

Thanks to the flexible nature of the many OH groups, these methylated monosaccharides can take on many different conformations. For a systematic search of low-energy minima, we utilized the CREST program (Conformer–Rotamer Ensemble Sampling Tool) by Grimme and co-workers.[16] Successful searches with other OH rich systems for rotational spectroscopic studies have been previously reported.[17] The CREST conformational searches yielded ~100 conformers per monosaccharide, in a 25 kJ mol^{-1} energy window. These conformers were then optimized at the B3LYP[18]-D3[19](BJ)[20]/def2-TZVP[21] level using Gaussian 16.[22] After optimization and harmonic frequency calculations, there are 6 conformers of Me-α-Glc, 7 conformers of Me-β-Glc, 8 conformers of Me-α-Gal and 11 conformers of Me-β-Glc within a 10 kJ mol^{-1} energy window. All theoretical details are summarized in Point S1, Supporting Information (SI). Spectroscopic parameters of low energy conformers are provided in Tables S1.1–S1.4, Point S1, SI.

The previously used conformational labelling scheme implemented for α-galactose[11] was adopted. While α and β are used to distinguish between anomers (highlighted with the red solid curves in Figure 1), the plausible torsional angles of −60°, +60°, and 180° are labelled as g–/G–, g+/G+, and t/T, respectively, where capitalization signifies that the torsional angle involves only heavy atoms. Generally, each conformer is labelled with three terms, for example, G+g–/cc/T. The first term describes Φ_1, the O6–C6–C5–O5 dihedral angle (Figure 1c), and Φ_2, the H6–O6–C6–C5 dihedral angle (Figure 1d). Next, the cooperative network of hydrogen bonds can take on clockwise (cl) or counterclockwise (cc) directions (Figure 1b.) The third term describes Φ_3, the CH3–O1–C1–C2 dihedral angle (Figure 1e.), corresponding to the orientation of the methoxy group at the anomeric carbon, C1. As shown in Tables S1.1–S1.4, almost all predicted low energy conformers adopt cc and T arrangements for the last

two labels and differ only in the configurations described by the first term.

Spectral Assignments and Conformer Identifications

The broadband rotational spectra of Me-α-Glc, Me-β-Glc, Me-α-Gal and Me-β-Gal were recorded using a 2–6 GHz CP-FTMW spectrometer[23] with the newly designed heated nozzle. All experimental details including the nozzle design are provided in Point S2, SI. An example spectrum of Me-β-Glc is depicted in Figure 2, and sections of the four recorded spectra are provided in Figure S3.1. These measurements demonstrate the general sensitivity achieved for this class of molecules, which is similar to that reported for other monosaccharides using the laser ablation approach coupled to a CP-FTMW instrument.[11]

In our experiments, the solid monosaccharide samples were placed inside the nozzle, heated and transferred into the gas phase, and finally expanded into the vacuum chamber through a supersonic jet expansion. This process prevents solvent-mediated interconversion between α- and β-anomers. We note that in aqueous solution and at neutral pH, methylated monosaccharides show negligible anomeric interconversion,[24] because the methoxy group at the anomeric carbon (C1) prevents the ring-chain tautomerism. Thus, we can assert that no α-/β-interconversion occurs before or during the jet expansion.

For Me–β-Glc (Figure 2), the rotational spectroscopic assignment began by recognizing that the predicted most stable conformer has a significant μ_a electric dipole component (3.4 D) which produces characteristic *a*-type spectral patterns. By comparing the experimental to the simulated spectrum, which is based on the predicted rotational constants, dipole moment components, and a rotational temperature of 1 K, 38 *a*-type transitions, some of which show methyl internal rotor splittings, were assigned. Two *b*-type and four *c*-type transitions were also identified later. After removing the assigned lines from the observed spectrum, we identified a second set of 44 *a*-type transitions, while no *b*-type or *c*-type transitions were found. Following the same procedure, a third set of 22 *a*-type transitions was assigned and again no related *b*- or *c*-type lines were identified. The assignments of the other monosaccharides followed a similar procedure, although with their own specific challenges, and are summarized in Point S3, SI.

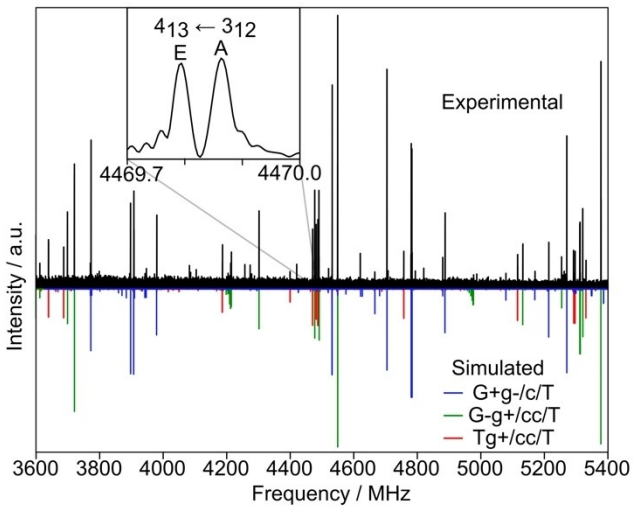

Figure 2. Experimental (top) and simulated (bottom) rotational spectrum of Me–β-Glc. The simulation contains the simulated spectra of three Me-β-Glc conformers: G-g+/cc/T (green), G+g-/cc/T (blue), and Tg+/cc/T (red). In the upper left box, the A and E species of the $4_{13} \leftarrow 3_{12}$ transition of Me-β-Glc, G-g+/cc/T are resolved and assigned. The resolved A and E species have allowed for the determination of the barrier height to methyl internal rotation. The experimental spectrum was taken with an accumulation of 580,000 free induction decays.

The assigned rotational transitions were fitted using Watson's A-reduction Hamiltonian in its I^r representation using the SPFIT/SPCAT program.[25] In several conformers, splittings associated with the internal rotation of the methyl rotor were observed (a topic which will be further explored below) and the spectroscopic fits were done using the XIAM program.[26]

To determine the carrier of each set of transitions, we considered the following three general criteria: 1) relative Gibbs free energy ordering of conformers at 423 K, the nozzle temperature, 2) agreement between experimental and computational rotational constants, and 3) agreement between relative experimental transition intensities and theoretical electric dipole moment components. This assignment rubric has been commonly applied to identify a particular conformer as the carrier in rotational spectroscopic studies, for example in the studies of 4,4,4-trifluoro-1-butanol and its hydrogen bonded dimer,[27] although relative zero-point corrected energies were typically used for the non-covalently bonded species because they are formed and stabilized at very low temperature. Finally, in some cases where methyl internal rotation splittings were observed, we also compared the experimental barriers to the theoretical ones for confirmation. With these considerations, we were able to conclusively identify six conformers of of Me-Glc and four of Me-Gal experimentally.

Below we summarize the conformational identification results for Me-α-Glc, Me-β-Glc, Me-α-Gal and Me-β-Gal. Figure 2 shows a comparison of the simulated spectra of the three assigned Me-β-Glc conformers with the experimental spectrum as an example. The experimental spectroscopic constants and the corresponding theoretical ones are summarized in Tables 1 and 2, and the corresponding experimental rotational transition frequencies are listed in Tables 3.1–3.10, Point S3, SI.

Me-α-Glc and Me-β-Glc. Me-α-Glc has three predicted conformers within a 1 kJ mol^{-1} window, all of which were observed experimentally (Table 1). These conformers differ in their O5–C5–C6–O6 dihedral angle as shown in Figure 3a, taking on the G+, G- and T configuration. Based on the above criteria, we were able to assign the carrier of the first set of experimental lines to the predicted lowest energy conformer, G+g-/cc/T, the second to G-g+/cc/T, which–at

Table 1. Experimental and predicted[a] spectroscopic parameters[b] of the observed conformers of Me-α-Glc and Me-β-Glc.

Me-α-Glc	G+g-/cc/T	G-g+/cc/T	Tg+/cc/T	G+g-/cc/T	G-g+/cc/T	Tg+/cc/T
A [MHz]	928.54628(60)[c]	919.49311(43)	979.9331(26)	921	916	980
B [MHz]	738.17176(47)	728.87715(34)	698.71425(33)	739	725	694
C [MHz]	464.37402(18)	490.48080(15)	459.82643(27)	462	487	457
$\lvert\mu_a, \mu_b, \mu_c\rvert$ [Debye]	$\mu_a \approx \mu_b$, no μ_c[d]	$\mu_a > \mu_b > \mu_c$	μ_a, no μ_b, no μ_c	1.6, 2.2, 0.1[d]	2.9, 2.1, 0.9	2.8, 0.4, 0.3
V_3 [kJ mol^{-1}]	—[e]	—	—	6.73	6.19	6.08
N/σ [kHz]	37/5.7	42/5.3	22/4.6	—	—	—
Me-β-Glc	G+g-/cc/T	G-g+/cc/T	Tg+/cc/T	G+g-/cc/T	G-g+/cc/T	Tg+/cc/T
A [MHz]	896.23064(46)[c]	815.90742(46)	978.96948(166)	895	814	983
B [MHz]	723.69503(19)	777.35769(22)	652.20614(20)	722	776	649
C [MHz]	440.15129(11)	414.73073(8)	408.35847(14)	439	414	407
$\lvert\mu_a, \mu_b, \mu_c\rvert$ [Debye]	$\mu_a > \mu_c \gg \mu_b$[d]	μ_a, no μ_b, no μ_c	μ_a, no μ_b, no μ_c	3.4, 0.1, 1.2	3.2, 0.6, 0.0	3.1, 0.8, 0.2
V_3 [kJ mol^{-1}]	6.456(6)	6.105(9)	6.53(1)	6.28	5.83	6.34
N/σ [kHz]	44/5.1	44/4.7	27/4.5	—	—	—

[a] Predicted at the B3LYP–D3(BJ)/def2-TZVP level. [b] *A*, *B* and *C* are the rotational constants, $\lvert\mu_a\rvert$, $\lvert\mu_b\rvert$, and $\lvert\mu_c\rvert$ are the absolute values of the electric dipole moment components, V_3 is the methyl internal rotation barrier, *N* is the number of the measured transitions included in the fit, and σ is the standard deviation of the fit. [c] Standard errors are shown in parentheses in units of the last digit. [d] Experimentally estimated relative magnitudes of $\lvert\mu_a\rvert$, $\lvert\mu_b\rvert$, and $\lvert\mu_c\rvert$. [e] The tunnelling splittings associated the methyl internal rotor were not resolved for a V_3 determination. Further discussion is provided in the section titled "Methyl Internal Rotation.

Table 2. Experimental and predicted[a] spectroscopic parameters[b] of the observed conformers of Me-α-Gal and Me-β-Gal.

Me-α-Gal	G+g-/cc/T	Tg+/cc/T	G+g-/cc/T	Tg+/cc/T
A [MHz]	972.14775(20)[c]	999.5174(26)	963	1008
B [MHz]	745.48408(13)	711.46844(41)	746	704
C [MHz]	472.356453(77)	470.24563(22)	470	466
$\lvert\mu_a, \mu_b, \mu_c\rvert$ [Debye]	$\mu_b > \mu_a \gg \mu_c$ [d]	μ_a, no μ_b, no μ_c no μ_b no μ_c	1.3, 2.2, 0.7[c]	2.5, 0.8, 0.6
V_3 [kJ mol^{-1}]	—[e]	—	6.761	6.168
N/σ [kHz]	45/3.2	13/3.1	—	—
Me-β-Gal	G+g-/cc/T	Tg+/cc/T	G+g-/cc/T	Tg+/cc/T
A [MHz]	866.80455(49)[c]	985.68575(258)	863	992
B [MHz]	760.37460(28)	674.29776(34)	760	671
C [MHz]	440.84315(10)	433.60421(21)	439	432
$\lvert\mu_a, \mu_b, \mu_c\rvert$ [Debye]	$\mu_a \approx \mu_b > \mu_c$	μ_a, no μ_b, no μ_c	2.0, 1.9, 0.8	2.8, 0.1, 0.6
V_3 [kJ mol^{-1}]	6.189(4)	—[e]	5.926	6.486
N/σ [kHz]	60/5.5	18/5.4	—	—

[a] Predicted at the B3LYP–D3(BJ)/def2-TZVP level. [b] *A*, *B* and *C* are the rotational constants, $\lvert\mu_a\rvert$, $\lvert\mu_b\rvert$, and $\lvert\mu_c\rvert$ are the absolute values of the electric dipole moment components, V_3 is the methyl internal rotation barrier, *N* is the number of the measured transitions included in the fit, and σ is the standard deviation of the fit. [c] Standard errors are shown in parentheses in units of the last digit. [d] Experimentally estimated relative magnitudes of $\lvert\mu_a\rvert$, $\lvert\mu_b\rvert$, and $\lvert\mu_c\rvert$. [e] The tunnelling splittings associated the methyl internal rotor were not resolved for a V_3 determination. Further discussion is provided in the section titled "Methyl Internal Rotation.

423 K–has a relative Gibbs free energy ($\Delta G_{423\,K}$) of 0.1 kJ mol^{-1}, and the third to Tg+/cc/T, which has with a relative $\Delta G_{423\,K}$ of 1.3 kJ mol^{-1}. These three observed conformers are analogous to the three most abundant conformers detected for α-Glc.[11] As can be seen in Figure 3a, all three conformers adopt a counterclockwise hydrogen bonding network. In fact, the lowest energy conformer of Me-α-Glc with a clockwise hydrogen bonding network has a relative $\Delta G_{423\,K}$ of 9.0 kJ mol^{-1} (Table S1.1.) Notably, in the unmethylated analogue, α-Glc, *one* of the observed conformers has a clockwise hydrogen bonding network,[10] highlighting the effect of methylation.

Similarly, Me-β-Glc also has three low-energy conformers, all of which were detected experimentally (see Table 1 and Figure 3b). The observed conformers of Me-β-Glc exhibit very similar intramolecular interaction patterns as those of Me-α-

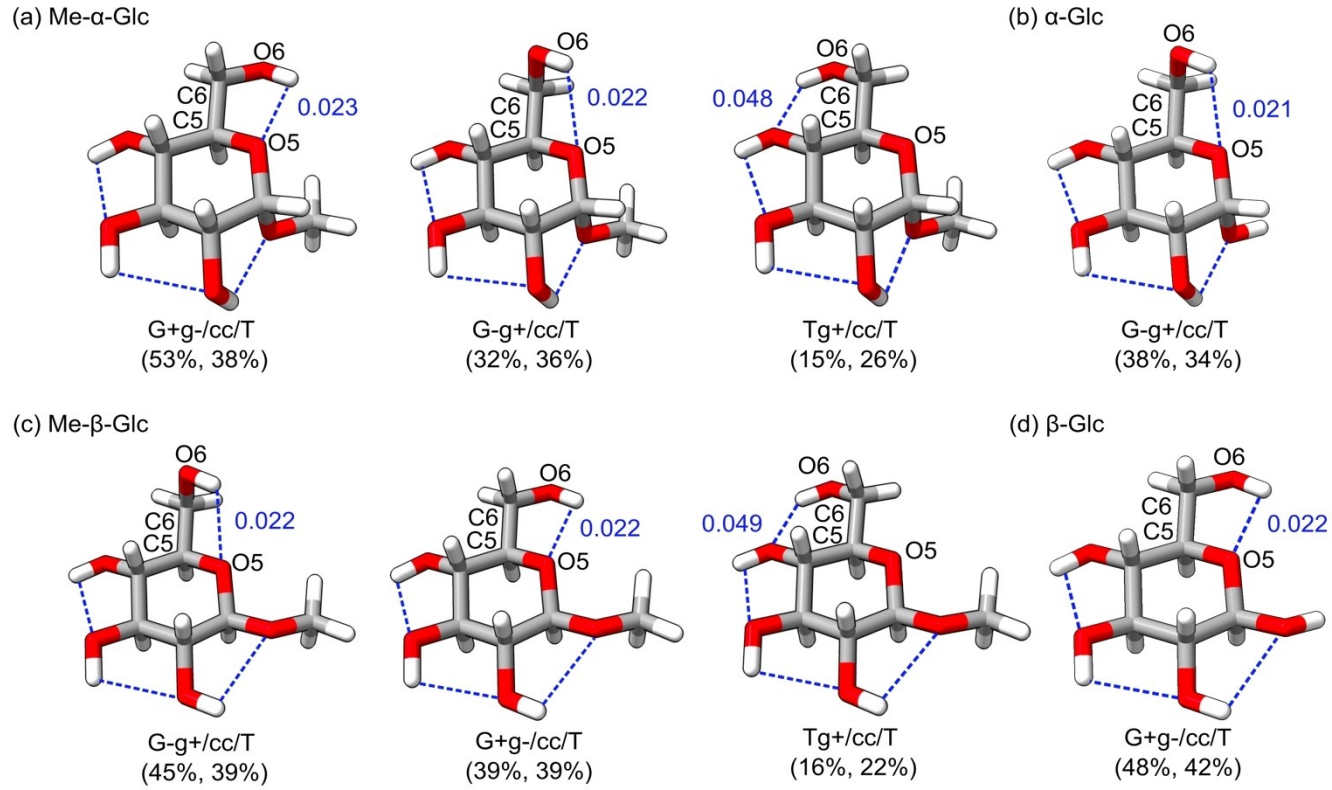

Figure 3. Optimized geometries of (a) Me-α-Gal conformers, (b) the most abundant conformer of of α-Glc, (c) Me-β-Glc conformers, and (d) the most abundant conformer of β-Glc. Experimental and theoretical percent abundances are given in parentheses, i.e., (exp. %, theo. %). The experimental abundances of the α-Glc and β-Glc conformers are from Ref.10. The theoretical abundances were calculated using $\Delta G_{423\,K}$ for the methylated monosaccharides and $\Delta G_{298\,K}$ for the unmethylated monosaccharides (see Point S4, SI). The hydrogen bond contacts are indicated by the dashed blue lines and the IBSI values associated with the O6H···O hydrogen bond contacts are provided. IBSI values for all intramolecular hydrogen bond contacts of Me-α-Glc and Me-β-Glc are provided in Point S6, SI and discussed later in the main text.

Glc, except that the most stable conformer switches from G+ g- to G-g+ (see Figure 3a and c). Comparing to Me–β-Glc's unmethylated analogue, β-Glc, analogous conformers were observed with comparable abundances, i.e., the same energy ordering.[10]

For the observed conformers, experimental percent abundances were estimated by comparing the relative intensities of *a*-type transitions with consideration of computed dipole moment components and a rotational temperature of 1 K. The simulated spectra of the three assigned conformers are shown in Figure 2. The experimental percent abundances are provided in Figure 3, together with the theoretical abundances calculated based on $\Delta G_{423\,K}$ (see Point S4, SI).

Me-α-Gal and Me-β-Gal Me-α-Gal differs from Me-α-Glc by its O4H hydroxyl group, which is positioned axially instead of equatorially. Experimentally, two conformers, G+g–/cc/T and Tg+/cc/T were identified, and their spectroscopic constants and geometries are given in Table 2 and Figure 4a, respectively. While identifying G+g-/cc/T was straightforward based on the criteria outlined above, both G-g-/cc/T and Tg+/cc/T were initially considered as the carrier of the second set of the transitions assigned for Me-α-Gal where only *a*-type transitions were measured. Upon closer inspection, one can see that G–g–/cc/T was predicted to have a sizable μ_c value of 2.2 Debye whereas Tg+/cc/T has a μ_c of 0.6 Debye. The former is inconsistent with the absence of *c*-type transitions. As well, the experimental rotational constants of Conformer II more closely match those predicted for Tg+/cc/T, supporting the final assignment listed in Table 2.

To rationalize the non-observation of G-g-/cc/T, we considered possible conformational cooling from G-g-/cc/T to the two observed conformers by constructing a 2D potential energy surface (PES) for Me-α-Gal and Me-β-Gal along two relevant dihedral angles at the B3LYP–D3(BJ)/def2-TZVP level. The resulting PESs are provided in Figure S5.2, Point S5, SI, while the definition of the two dihedral angles is shown in Figure S5.1. For completeness, the related PESs for Me-α-Glc and Me-β-Glc are also included in Figure S5.2. The interconversion barriers to G+g–/cc/T and Tg+/cc/T are predicted to be ~23 and ~11 kJ mol^{-1}, respectively, much higher than the empirical barrier of ~4.8 kJ mol^{-1}[28] for effective cooling. Additionally, it is necessary to consider the conversion path (i.e., barrier width) when discussing the probability of conversion. This is illustrated by the recent study of cis-1,2-cyclohexanediol, where a high energy conformer, **III**, was still observed in both helium and neon expansions due to its large barrier width, even though the conversion barrier is only ~3.7 kJ mol^{-1}.[17b] The very high predicted barriers (with uncertainties likely no more than a

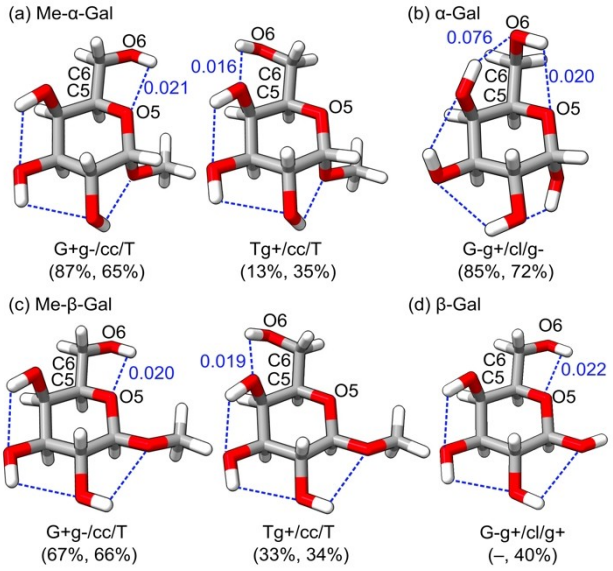

Figure 4. Optimized geometries of (a) Me-α-Gal conformers, (b) the most abundant conformer of α-Gal, (c) Me-β-Gal conformers, and (d) the most abundant conformer of β-Gal. Experimental and theoretical percent abundances are given in parentheses, i.e., (exp. %, theo. %). The experimental abundance of the α-Gal conformer is from Ref. [11] and β-Gal has not yet been investigated by rotational spectroscopy. The theoretical abundances were calculated using $\Delta G_{423\,K}$ for the methylated monosaccharides and $\Delta G_{298\,K}$ for the unmethylated monosaccharides (see Point S4, SI). The hydrogen bond contacts are indicated by the dashed blue lines and the IBSI values associated with the O6H···O hydrogen bond contacts are provided. In the case of α-Gal and β-Gal, the IBSI value of OH···O6 is also given. IBSI values for all intramolecular hydrogen bond contacts of Me-α-Gal and Me-β-Gal are provided in Point S6, SI and discussed later in the main text.

few kJ mol^{-1}) and the considerable dihedral angle changes (see Figure S5.2) suggest that conformational relaxation is not the primary cause for the non-observation of G-g-/cc/T. Since the transitions of Tg+/cc/T were already fairly weak, it is most likely that G-g-/cc/T is not abundant enough in the molecular expansion to be detected.

Contrary to the observed conformers of Me-α-Gal, the most abundant conformer of α-Gal has a clockwise hydrogen bonding network (Figure 4b).[11] This comparison once again demonstrates the significant effect methylation can have on the conformational landscape of a monosaccharide, as discussed later.

As with Me-α-Gal, two low-energy conformers, G+g–/cc/T and Tg+/cc/T, were identified for Me-β-Gal (Table 2 and Figure 4c). Efforts to assign G–g–/cc/T were not successful. As in the case of Me-α-Gal, conformational cooling from G–g–/cc/T to the two observed conformers was ruled out by a 2D PES, showing barriers of 23 and 13 kJ mol^{-1} (Figure S5.2, SI) from G–g–/cc/T to G+g–/cc/T and G–g–/cc/T to Tg+/cc/T, respectively. G–g–/cc/T was not observed mainly as a consequence of its lower abundance as demonstrated by a $\Delta G_{423\,K}$ value of 1.7 kJ mol^{-1} relative to Tg+/cc/T (Table S4.1). Notably, we observe a switch in the directionality of the hydrogen bonding network upon methylation of Me-α-Gal from clockwise in the unmethylated conformer to counterclockwise in the methylated ones (Figure 4a and b).

We note that the unmethylated analogue of Me-β-Gal, β-Gal, has not yet been studied by rotational spectroscopy. In Figure 4c and d, the geometries of the observed Me-β-Gal conformers are compared with that of the computed, lowest energy conformer of β-Glc.

Methyl Internal Rotation In the assignments of the rotational spectra of the methylated glucoses and galactoses, splittings of rotational transitions were observed. Each rotational level splits into a non-degenerate A level and a doubly degenerate E level due to methyl rotor tunnelling, resulting in an equal intensity doublet.[29] Such splittings were observed in all four monosaccharide spectra and were utilized to determine the barrier heights of the methyl internal rotation whenever possible. For G+g-/cc/T, G-g+/cc/T, Tg+/cc/T of Me-β-Glc, and G+g-/cc/T of Me-β-Gal, experimental barrier heights were determined and their values are given in Tables 1 and 2. Generally, the experimental barrier heights are well predicted by theory, with the largest deviation from experiment being about 7%.

Even though the predicted barrier heights of all observed conformers are very similar, not all rotational spectra exhibit similar magnitudes of hyperfine splittings. For example, rotational transitions of G+g-/cc/T, G-g+/cc/T, and Tg+/cc/T of Me-α-Glc, G+g-/cc/T and Tg+/cc/T of Me-α-Glc, and Tg+/cc/T of Me-β-Gal exhibit too few resolved splittings for their methyl internal rotation barrier heights to be determined. This may sound contradictory in the first instance. However, such outcomes are exactly predicted using the theoretical barriers and the geometries of the specific conformers by XIAM. This is because the magnitude of the splittings depends not only on the barrier height but also on the position and orientation of the methyl group relative to the principal axes of the molecule. We used this observation to further verify the conformational assignments.

Instead of the equal intensity doublets, some peculiar mirror-imaged patterns, as shown in Figure 5, were also detected for example in G-g+/cc/T of Me-β-Glc. Since G-g+/cc/T of Me-β-Glc has $\mu_b = 0.1$ Debye and $\mu_a = 2.8$ Debye, one would expect *b*-type transitions, such as 5_{05}-4_{14} and 5_{15}-4_{04}, to

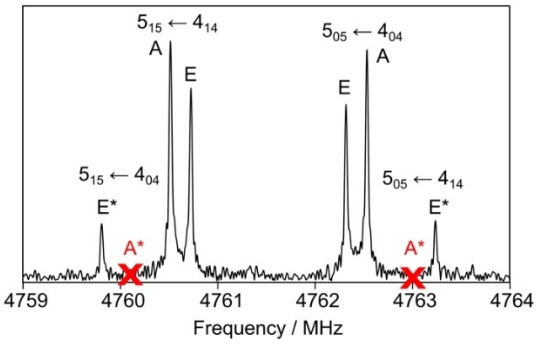

Figure 5. Examples of the unusual methyl internal rotor splittings of G-g+/cc/T of Me–β-Glc. The red 'X' designates the predicted position of the A* species. See text for further details.

be about a thousand times weaker than the related *a*-type transitions, such as 5_{05}-4_{04} and 5_{15}-4_{14}, and they would therefore not be present prominently in the same spectrum, in contrast to what is demonstrated in Figure 5. The drastic enhancement of the E* species lines of the 5_{15}-4_{04} and 5_{05}-4_{14} *b*-type transitions, as seen in Figure 5 is surprising. A detailed literature review revealed that such peculiar internal rotation splitting patterns were researched by Dreizler and co-workers[30] and more recently by Nguyen and co-workers.[31] For example, in the study of cis propionyl fluoride, Scappini and Dreizler showed that for two near degenerate *K*-doublet rotational levels, the A-species behave normally, whereas the E-species are affected by odd order terms in the Hamiltonian in the presence of a coupling between internal rotor and over-all rotation (see Equation (2) in Ref. [29a])). As a result, the original pair of the E-species wave functions mix and the asymmetric-rigid rotor selection rules break down, leading to the observation of the E* component of the "forbidden" rotational transitions. In our case, the sum of the 5_{05}-4_{14} E* line and 5_{05}-4_{04} E line intensities equals roughly that of the 5_{05}-4_{04} A line, and the "forbidden" *b*-type E* species line borrows intensity from the related *a*-type E species line. Although such effects were mainly observed in higher *K* transition previously, the current splitting pattern was correctly predicted by the XIAM program,[25] confirming its cause.

Hydrogen Bonding and Hyperconjugation: Competing Influences

The current rotational spectroscopic study clearly identifies the shapes of the most stable conformers (Figures 3 and 4) of the four monosaccharides. To gain further insights into how these conformational preferences come about, we employed several analysis tools including the non-covalent interaction (NCI) analysis,[32] the intrinsic bond strength index (IBSI),[33] and natural bond order (NBO)[34,35] analysis to unveil the physical origins of the preferences.

First, we examine whether intramolecular non-covalent interactions are responsible for the observed conformational preferences. The NCI plots of all the observed conformers are provided in Figure S6.1, Point S6, SI, while the related IBSI results are summarized in Figure S6.2. Based on the NCI and IBSI analyses, one can see that all observed conformers have four intramolecular hydrogen-bonding contacts. As shown in Figure 3, among the three low energy conformers of Me-α-Glc (Me-β-Glc), Tg+/cc/T has the strongest intramolecular hydrogen bond contact (O6H···O) with an IBSI index of 0.048 (0.049). For reference, the intermolecular hydrogen bond between two water molecules has an IBSI index of 0.084.[32] On the other hand, Tg+/cc/T is the least abundant conformer of Me-α-Glc and of Me-β-Glc detected experimentally. Clearly, considering only the electrostatic intramolecular interactions via electron density gradients is not sufficient to explain the conformer stability ordering.

Next, we applied hyperconjugation, a model which involves electron delocalization via the overlap of a σ-orbital with a σ*-, π*-, or p-orbital to rationalize conformational preferences.[36] Using second-order perturbation theory, as implemented in the NBO program, the stabilization energies of various orbital overlaps, also referred to as $E^{(2)}$ energies, were estimated (larger $E^{(2)}$ values indicate greater stability.) Due to the variations in orbital proximity and orientations, stabilization energies vary across conformers. The geometry that allows for favorable overlap, where the 'best donor' NBO is aligned with the 'best acceptor' NBO, yields the greatest stabilization energy.

To understand conformational preferences, orbital interactions between adjacent (vicinal) bonds are especially significant. These hyperconjugative interactions can be weakened or strengthened by rotation about a single bond. In our case, rotation about the C5–C6 bond gives rise to the G+, G-, and T conformers (the first letter in the naming scheme), each with a different spatial arrangement of orbitals. On both sides of the C5–C6 bond, there are three donor σ-orbitals (2 $\sigma_{C6\text{-}H}$, $\sigma_{C6\text{-}O6}$ on one side; $\sigma_{C5\text{-}H}$, $\sigma_{C5\text{-}C4}$, $\sigma_{C5\text{-}O5}$ on the other), each of which can donate to three acceptor σ*-orbitals on the opposing side (see Figure 6). This results in a total of 18 hyperconjugative interactions (3 donor orbitals ×3 acceptor orbitals ×2 sides = 18 vicinal interactions). The sum of the 18 corresponding stabilization energies allows us to determine which conformations are preferred by hyperconjugation. In the case of Me-α-Glc and Me-β-Glc, the G+ and G- conformers are preferred by hyperconjugation (see 'relative sum' in Table S7.1, Point S7, SI.)

The influence of hyperconjugation is nicely illustrated by considering the three observed conformers of Me-α-Glc and Me-β-Glc, shown in Figure 6. Unlike the T conformers, the G+ and G- conformers allow for stabilizing electron delocalization from $\sigma_{C\text{-}H}$ orbitals to $\sigma^*_{C\text{-}O}$ orbitals. This overlap yields a large stabilization energy because the $\sigma_{C\text{-}H}$ and $\sigma_{C\text{-}C}$ orbitals are good donors and the $\sigma^*_{C\text{-}O}$ orbitals are good acceptors. Analogously, the $\sigma^*_{C\text{-}O}$ orbital is a better electron acceptor than the $\sigma^*_{C\text{-}H}$ and $\sigma^*_{C\text{-}C}$ orbitals.

In case of the G+ and G- conformers, hyperconjugation outweighs the strong hydrogen bond interactions present in the T conformers. Stabilization energies for the 18 vicinal hyperconjugative interactions along the C5–C6 bond are summarized in Table S7.1, Point S7, SI.

This preference for the gauche configurations, such as G+ and G, is also known as the gauche effect and has previously

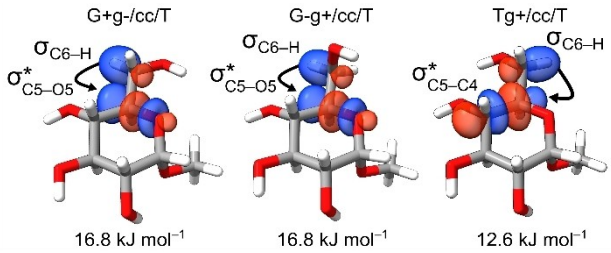

Figure 6. Comparison of two hyperconjugative interactions, $\sigma_{C6-H} \rightarrow \sigma^*_{C5-O5}$ and $\sigma_{C6-H} \rightarrow \sigma^*_{C5-C4}$, for the observed conformers of Me-α-Glc. The corresponding $E^{(2)}$ energies for each interaction are given below each conformer. The black arrow signifies the donor acceptor relationship. The selected interactions are just two of the 18 hyperconjugative interactions along the C5–C6 bond, the remaining interaction energies are listed in Table S7.1, Point S7, SI. The atom numbering can be found in Figure 3.

been investigated for a variety of systems.[35,37] The NBO results for Me–α-Glc and Me–β-Glc agree with the previous comment that hyperconjugation drives the gauche effect.[10,38] While NCI and IBSI analyses are widely used in conformational evaluations, these methods are mainly based on the electron density topology, and the importance of electron delocalization is often neglected. Me–α-Glc and Me–β-Glc exemplify the importance of considering electron delocalization when explaining conformational preferences.

On the other hand, the gauche effect cannot explain finer nuances. For example, it does not differentiate between G+ and G- or include temperature effects explicitly.[35] In the cases of Me-α-Gal and Me-β-Gal, the stability of T lies between G+ and G-, which cannot be rationalized with the gauche effect. To explain the observed conformer stabilities of Me-α-Gal and Me-β-Gal, it is necessary to consider the contribution of entropy and apply the relative Gibbs free energies (Point S4, SI). As demonstrated in Figures 3 and 4, this consideration explains the observed stability ordering of conformers for all four monosaccharides satisfactorily. The current gas-phase data of the four monosaccharides in isolated states, i.e., without solvent interference, provide important experimental benchmarks for theories investigating the origins of gauche effect, which remain a subject of ongoing debate.[35,36b,39]

The Impact of Methylation on Conformational Landscape

All observed conformers of the four monosaccharides exhibit a counterclockwise hydrogen bonding network, differing from the unmethylated analogues where clockwise hydrogen bonding networks are prevalent.[10,11] For example, the most abundant conformer of α-Gal has a clockwise network (Figure 4b). In contrast, the most stable clockwise conformer of Me–α–Gal could not be observed experimentally because of its high relative energy. Similarly, one of the observed conformers of α-Glc has a clockwise hydrogen bonding network,[10] whereas in the methylated analogue, Me–α-Glc, the clockwise hydrogen bonding network conformer is 10.1 kJ mol^{-1} less stable than the global minimum at 423 K (Table S1.3)

This switch from clockwise to counterclockwise hydrogen bonding networks upon methylation illustrates how substitutions at the anomeric carbon can affect the conformational landscape of a monosaccharide. In glucose and galactose, O1H can act as a hydrogen bond donor or acceptor to the neighbouring O2H. The presence of an O1–H···O2 interaction is critical in driving the preference for a clockwise hydrogen bonding network (Figure 4b and d). Replacing O1H with O1CH$_3$ prevents this critical hydrogen bond from forming because the anomeric substituent can no longer act as a hydrogen bond donor. Consequently, clockwise hydrogen bonding networks become energetically unfavorable, leading to the dominance of counterclockwise networks in the conformational landscapes of methylated monosaccharides.

The impact of methylation on the preferred orientation of the hydrogen bonding network emphasizes the effect of substitution at the anomeric carbon. In UV spectroscopic studies, it has often been assumed that substitutions at the anomeric carbon are 'structurally benign'.[40] This assumption allows for the incorporation of necessary UV chromophores, often phenyl substituents. Contrary to this assumption, we have found that methylation can impact the preferred orientation of the hydrogen bonding network, illustrating the potential effects of substitution at the anomeric carbon on conformational preferences. The current study highlights the potential pitfalls of using chromophores in conformational analyses.

Conclusions

This study is the first experimental investigation of the gas-phase, unbiased structures of the α and β anomers of two monosaccharides, Me-Glc and Me-Gal. Using CP-FTMW spectroscopy, we identified three distinct conformers each for Me-α-Glc and Me-β-Glc, and two each for Me-α-Gal and Me-β-Gal. Notably, these results were achieved without the need for an expensive and complicated laser ablation system, providing a methodological advancement in the CP-FTMW study of carbohydrates. In addition to establishing the conformational stability orderings of these complex monosaccharides, the study also explores the dynamics of methyl internal rotation motions and provides the associated experimental barriers.

Our results reveal the profound impact of methylation on the conformational behavior of these monosaccharides. In galactose, 1-O-methylation induces a drastic reorientation of the hydrogen bonding network, illustrating how small chemical modifications can significantly alter intramolecular interaction patterns. For Me–Glc, the interplay between hydrogen bonding and hyperconjugation underscores the significant role of hyperconjugative interactions in determining conformational preferences.

These experimental insights provide essential data for benchmarking theoretical models, which aim to predict the net impact of compounding stereoelectronic effects. Our work illustrates that, even in gas-phase systems, a single model, such as hyperconjugation, cannot fully explain the observed conformational stability ordering. Overall, this study provides new insights into the conformational preferences of monosaccharides and the multiple factors influencing them, and also high-quality experimental data for benchmarking future theoretical exploration of the origins of the gauche effect.

Supporting Information Summary

Point S1: theoretical methods, conformational search results, spectroscopic properties of low energy conformers, and Cartesian coordinates for the observed conformers. **Point S2**: experimental conditions and details pertaining to the newly designed pulsed nozzle cap. **Point S3**: example spectra, spectroscopic assignment details, and experimental transition frequency lists. **Point S4**: thermochemistry results at the nozzle temperature. **Point S5**: 2D relaxed potential energy surface scans for interconversion barriers between conformers. **Point**

S6: NCI and IBSI analyses. **Point S7**: NBO analyses of hyperconjugative interactions.

The authors have cited additional references within the Supporting Information.[41–47]

Acknowledgements

This work was funded by the Natural Sciences and Engineering Research Council (NSERC) of Canada and by the University of Alberta. We gratefully acknowledge access to the computing facilities by the Shared Hierarchical Academic Research Computing Network (SHARCNET), the Western Canada Research Grid (Westgrid), the Digital Research Alliance of Canada, and Centro de Super Computación de Galicia (CESGA) of Spain. JCW thanks NSERC for an undergraduate summer research award and Gilead Sciences for the IDChem award. AI thanks the Basque Government for a postdoctoral fellowship. ASH acknowledges the support from Alberta Graduate Excellence Scholarships and Marshall Syska Graduate Scholarships. YX is a Tier 1 Canada Research Chair in Chirality and Chirality Recognition.

Conflict of Interests

The authors declare no conflict of interest.

Data Availability Statement

The data that support the findings of this study are available in the supplementary material of this article.

Keywords: Rotational spectroscopy · Conformation analysis · Hyperconjugation · Hydrogen bonding · Monosaccharides

[1] T. K. Lindhorst, *Essentials of Carbohydrate Chemistry and Biochemistry*, John Wiley & Sons, Weinheim **2007**.
[2] C. M. McMahon, C. R. Isabella, I. W. Windsor, P. Kosma, R. T. Raines, L. L. Kiessling, *J. Am. Chem. Soc.* **2020**, *142*, 2386–2395.
[3] a) P.-S. Tseng, C. Ande, K. W. Moremen, D. Crich, *Angew. Chem. Int. Ed.* **2023**, *135*, e202217809; b) S. Bertuzzi, A. Gimeno, R. Núñez-Franco, G. Bernardo-Seisdedos, S. Delgado, G. Jiménez-Osés, O. Millet, J. Jiménez-Barbero, A. Ardá, *Chem. Eur. J.* **2020**, *26*, 15643–15653; c) M. G. Lete, M. Hoffmann, N. Schomann, A. Martínez-Castillo, F. Peccati, P. B. Konietzny, S. Delgado, N. L. Snyder, G. Jiménez-Oses, N. G. A. Abrescia, A. Ardá, L. Hartmann, J. Jiménez-Barbero, *ACS Omega* **2023**, *8*, 16883–16895.
[4] Y. Yu, M. Delbianco, *Chem. Eur. J.* **2020**, *26*, 9814–9825.
[5] a) S. Perez, O. Makshakova, *Chem. Rev.* **2022**, *122*, 15914–15970; b) X. S. Streety, J. C. Obike, S. D. Townsend, *ACS Cent. Sci.* **2023**, *9*, 1285–1296.
[6] a) M. Marianski, A. Supady, T. Ingram, M. Schneider, C. Baldauf, *J. Chem. Theory Comput.* **2016**, *12*, 6157–6168; b) L. Kong, R. A. Bryce, *J. Comput. Chem.* **2022**, *43*, 2009–2022.
[7] I. V. Alabugin, G. dos Passos Gomes, M. A. Abdo, *WIREs Comput. Mol. Sci.* **2019**, *9*, e1389.
[8] a) C. B. Park, R. W. Field, *J. Chem. Phys.* **2016**, *144*, 200901; b) G. G. Brown, B. C. Dian, K. O. Douglass, S. M. Geyer, S. T. Shipman, B. H. Pate, *Rev. Sci. Instrum.* **2008**, *79*, 053103.
[9] a) J. Thomas, X. Liu, W. Jäger, Y. Xu, *Angew. Chem. Int. Ed.* **2015**, *54*, 11711–11715; *Angew. Chem.* **2015**, *127*, 11877–11881; b) Z. Su, Y. Xu, *Angew. Chem. Int. Ed.* **2007**, *46*, 6163–6166; *Angew. Chem.* **2007**, *119*.
[10] a) F. Xie, X. Ng, N. A. Seifert, J. Thomas, W. Jäger, Y. Xu, *J. Chem. Phys.* **2018**, *149*, 224306; b) J. Thomas, E. Mariona, Y. Xu, *J. Chem. Phys.* **2017**, *146*, 104303.
[11] J. L. Alonso, M. A. Lozoya, I. Peña, J. C. López, C. Cabezas, S. Mata, S. Blanco, *Chem. Sci.* **2014**, *5*, 515–522.
[12] I. Peña, C. Cabezas, J. L. Alonso, *Chem. Commun.* **2015**, *51*, 10115–10118.
[13] G. Juárez, E. R. Alonso, M. Sanz-Novo, J. L. Alonso, I. León, *Phys. Chem. Chem. Phys.* **2022**, *24*, 23076–23081.
[14] C. Calabrese, I. Uriarte, A. Insausti, M. Vallejo-López, F. J. Basterretxea, S. A. Cochrane, B. G. Davis, F. Corzana, E. J. Cocinero, *ACS Cent. Sci.* **2020**, *6*, 293–303.
[15] a) L. Petitpoisson, A. Pichette, J. Alsarraf, *Org. Chem. Front.* **2022**, *9*, 5414–5425; b) S. M. Muthana, C. Campbell, J. C. Gildersleeve, *ACS Chem Biol* **2012**, *7*, 31–43.
[16] a) S. Spicher, S. Grimme, *Angew. Chem. Int. Ed.* **2020**, *59*, 15665–15673; *Angew. Chem.* **2020**, *132*, 15795–15803; b) P. Pracht, F. Bohle, S. Grimme, *Phys. Chem. Chem. Phys.* **2020**, *22*, 7169–7192.
[17] a) A. S. Hazrah, A. Insausti, J. Ma, M. H. Al-Jabiri, W. Jäger, Y. Xu, *Angew. Chem. Int. Ed.* **2023**, *62*, e202310610; b) J. Ma, A. Insausti, M. H. Al-Jabiri, C. D. Carlson, W. Jäger, Y. Xu, *J. Chem. Phys.* **2024**, *160*, 154304.
[18] a) A. D. Becke, *J. Chem. Phys.* **1993**, *98*, 5648–5652; b) P. J. Stephens, F. J. Devlin, C. F. Chabalowski, M. J. Frisch, *J. Phys. Chem.* **1994**, *98*, 11623–11627.
[19] S. Grimme, S. Ehrlich, L. Goerigk, *J. Comput. Chem.* **2011**, *32*, 1456–1465.
[20] A. D. Becke, E. R. Johnson, *J. Chem. Phys.* **2005**, *123*, 154101.
[21] a) F. Weigend, R. Ahlrichs, *Phys. Chem. Chem. Phys.* **2005**, *7*, 3297; b) A. Schäfer, C. Huber, R. Ahlrichs, *J. Chem. Phys.* **1994**, *100*, 5829–5835.
[22] M. J. Frisch, G. W. Trucks, H. B. Schlegel, G. E. Scuseria, M. A. Robb, J. R. Cheeseman, G. Scalmani, V. Barone, G. A. Petersson, H. Nakatsuji, X. Li, M. Caricato, A. V. Marenich, J. Bloino, B. G. Janesko, R. Gomperts, B. Mennucci, H. P. Hratchian, J. V. Ortiz, A. F. Izmaylov, J. L. Sonnenberg, D. Williams-Young, F. Ding, F. Lipparini, F. Egidi, J. Goings, B. Peng, A. Petrone, T. Henderson, D. Ranasinghe, V. G. Zakrzewski, J. Gao, N. Rega, G. Zheng, W. Liang, M. Hada, M. Ehara, K. Toyota, R. Fukuda, J. Hasegawa, M. Ishida, T. Nakajima, Y. Honda, O. Kitao, H. Nakai, T. Vreven, K. Throssell, J. A. Montgomery, Jr., J. E. Peralta, F. Ogliaro, M. J. Bearpark, J. J. Heyd, E. N. Brothers, K. N. Kudin, V. N. Staroverov, T. A. Keith, R. Kobayashi, J. Normand, K. Raghavachari, A. P. Rendell, J. C. Burant, S. S. Iyengar, J. Tomasi, M. Cossi, J. M. Millam, M. Klene, C. Adamo, R. Cammi, J. W. Ochterski, R. L. Martin, K. Morokuma, O. Farkas, J. B. Foresman, D. J. Fox, *Gaussian 16, Revision C.01*, Gaussian, Inc., Wallingford CT **2016**.
[23] a) N. A. Seifert, J. Thomas, W. Jäger, Y. Xu, *Phys. Chem. Chem. Phys.* **2018**, *20*, 27630–27637; b) F. Xie, N. A. Seifert, W. Jäger, Y. Xu, *Angew. Chem. Int. Ed.* **2020**, *59*, 15703–15710; *Angew. Chem.* **2020**, *132*,15833–15840.
[24] K. B. Wiberg, M. Marquez, *J. Am. Chem. Soc.* **1994**, *116*, 2197–2198.
[25] H. M. Pickett, *J. Mol. Spectrosc.* **1991**, *148*, 371–377.
[26] H. Hartwig, H. Dreizler, *Z. Naturforsch. A.* **1996**, *51*, 923–932.
[27] a) T. Lu, F. Xie, N. A. Seifert, R. Hamidi Mejlej, W. Jäger, Y. Xu, *Phys. Chem. Chem. Phys.* **2024**, *16*, 10538–10545; b) T. Lu, F. Xie, N. A. Seifert, W. Jäger, Y. Xu, *J. Mol. Struct.* **2020**, *1217*, 128359/1–12.
[28] R. S. Ruoff, T. D. Klots, T. Emilsson, H. S. Gutowsky, *J. Chem. Phys.* **1990**, *93*, 3142–3150.
[29] a) C. C. Lin, J. D. Swalen, *Rev. Mod. Phys.* **1959**, *31*, 841–892; b) D. R. Herschbach, J. D. Swalen, *J. Chem. Phys.* **1958**, *29*, 761–776; c) N. L. Owen, G. Ole. Soerensen, *J. Phys. Chem.* **1979**, *83*, 1483–1488; d) J. T. A. Gall, J. Thomas, F. Xie, Z. Wang, W. Jäger, Y. Xu, *Phys. Chem. Chem. Phys.* **2017**, *19*, 29508–29515; e) H. V. L. Nguyen, W. Caminati, J.-U. Grabow, *Molecules.* **2022**, *27*, 3948.
[30] a) F. Scappini, H. Dreizler, *Z. Naturforsch. A.* **1981**, *36*, 1327–1333; b) G. Bestmann, W. Lalowski, H. Dreizler, *Z. Naturforsch. A.* **1985**, *40*, 271–273; c) H. Hartwig, H. Dreizler, *Z. Naturforsch. A.* **1992**, *47*, 1051–1057.
[31] N.-N. Dang, H.-N. Pham, I. Kleiner, M. Schwell, J.-U. Grabow, H. V. L. Nguyen, *Molecules.* **2022**, *27*, 2639.
[32] Á. Sánchez-González, P. Grenut, A. Gil, *J. Comput. Chem.* **2022**, *43*, 804–821.
[33] J. Klein, H. Khartabil, J.-C. Boisson, J. Contreras-García, J.-P. Piquemal, E. Hénon, *J. Phys. Chem. A.* **2020**, *124*, 1850–1860.
[34] B. Cao, C. Wang, Z. Zhou, *Carbohydr. Res.* **2023**, *523*, 108738.
[35] E. D. Glendening, J. K. Badenhoop, A. E. Reed, J. E. Carpenter, J. A. Bohmann, C. M. Morales, P. Karafiloglou, C. R. Landis, F. Weinhold, *NBO 7.0.*, Theoretical Chemistry, Institute University of Wisconsin, Madison **2018**.
[36] a) R. C. Ferreira, *J. Chem. Educ.* **1952**, *29*, 554; b) J. J. Mullins, *J. Chem. Educ.* **2012**, *89*, 834–836; c) I. V. Alabugin, L. Kuhn, N. V. Krivoshchapov, P. Mehaffy, M. G. Medvedev, *Chem. Soc. Rev.* **2021**, *50*, 10212–10252.

[37] a) C. Thiehoff, Y. P. Rey, R. Gilmour, *Isr. J. Chem.* **2017**, *57*, 92–100; b) D. Rodrigues Silva, L. de Azevedo Santos, T. A. Hamlin, C. Fonseca Guerra, M. P. Freitas, F. M. Bickelhaupt, *ChemPhysChem* **2021**, *22*, 641–648.
[38] S. Wolfe, *Acc. Chem. Res.* **1972**, *5*, 102–111.
[39] K. N. Kirschner, R. J. Woods, *PNAS* **2001**, *98*, 10541–10545.
[40] a) P. Çarçabal, R. A. Jockusch, I. Hünig, L. C. Snoek, R. T. Kroemer, B. G. Davis, D. P. Gamblin, I. Compagnon, J. Oomens, J. P. Simons, *J. Am. Chem. Soc.* **2005**, *127*, 11414–11425; b) S. Daly, F. Poussigue, A.-L. Simon, L. MacAleese, F. Bertorelle, F. Chirot, R. Antoine, P. Dugourd, *Anal. Chem.* **2014**, *86*, 8798–880; c) S. Bakels, M.-P. Gaigeot, A. M. Rijs, *Chem. Rev.* **2020**, *120*, 3233–3260.
[41] C. Bannwarth, S. Ehlert, S. Grimme, *J. Chem. Theo. Comput.* **2019**, *15*, 1652–1671.
[42] F. O. Talbot, J. P. Simons, *Phys. Chem. Chem. Phys.* **2002**, *4*, 3562–3565.
[43] N. Borho, Y. Xu, *Phys. Chem. Chem. Phys.* **2007**, *9*, 1324–1328.
[44] T. Lu, F. Chen, *J. Comput. Chem.* **2012**, *33*, 580–592.
[45] E. F. Pettersen, T. D. Goddard, C. C. Huang, E. C. Meng, G. S. Couch, T. I. Croll, J. H. Morris, T. E. Ferrin, *Protein Sci.* **2021**, *30*, 70–82.
[46] A. J. Schaefer, V. M. Ingman, S. E. Wheeler, *J. Comput. Chem.* **2021**, *42*, 1750–1754.
[47] C. M. Western, *J. Quant. Spectrosc. Radiat. Transf.* **2017**, *186*, 221–242.

Manuscript received: August 23, 2024
Accepted manuscript online: September 23, 2024
Version of record online: November 18, 2024